Published in final edited form as:

Nat Struct Mol Biol. ; 19(1): 40–47. doi:10.1038/nsmb.2162.

Intrinsic tethering activity of endosomal Rab proteins

Sheng-Ying Lo[1,2], **Christopher L. Brett**[1,3], **Rachael L. Plemel**[1], **Marissa Vignali**[4], **Stanley Fields**[4,5], **Tamir Gonen**[1,5,6], and **Alexey J. Merz**[1]

[1]Department of Biochemistry, University of Washington School of Medicine, Seattle WA 98195

[2]Department of Chemistry, University of Washington School of Medicine, Seattle WA 98195

[4]Department of Genome Sciences, University of Washington School of Medicine, Seattle WA 98195

[5]Howard Hughes Medical Institute, University of Washington School of Medicine, Seattle WA 98195

Abstract

Rab small G-proteins control membrane trafficking events required for a multitude of processes including secretion, lipid metabolism, antigen presentation, and growth factor signaling. Rabs recruit effectors that mediate diverse functions including vesicle tethering and fusion. However, many mechanistic questions about Rab-regulated vesicle tethering are unresolved. Using chemically defined reaction systems we discovered that Vps21, a *Saccharomyces cerevisiae* ortholog of mammalian endosomal Rab5, functions *in trans* with itself and with at least two other endosomal Rabs to directly mediate GTP-dependent tethering. Vps21-mediated tethering was stringently and reversibly regulated by an upstream activator, Vps9, and an inhibitor, Gyp1, which were sufficient to drive dynamic cycles of tethering and de-tethering. These experiments reveal an unexpected mode of tethering by endocytic Rabs. In our working model, the intrinsic tethering capacity Vps21 operates in concert with conventional effectors and SNAREs to drive efficient docking and fusion.

Vesicle and organelle tethering are reversible recognition events that precede docking and bilayer fusion. Tethering also mediates transient contacts that allow materials such as lipids to be passed between organelles [1]. The most broadly deployed regulators of tethering are small G-proteins of the Rab and Arf families[2,3]. These molecular switches, inactive when GDP-bound, become activated upon GTP binding. Rabs are activated by guanosine

Please address correspondence to Alex Merz: merza@uw.edu, +1-206-616-8308, www.merzlab.org.

[3]Current address: Department of Biology, Concordia University, Montreal, Quebec H4B 1R6

[6]Current address: Janelia Farm Research Campus, Howard Hughes Medical Institute, Ashburn, VA 20147

AUTHOR CONTRIBUTIONS

S.-Y.L. and A.M. conceived the project. S.-Y.L. developed and validated the QLS-based tethering system; expressed, purified, and characterized proteins; prepared liposomes, and performed and interpreted all QLS tethering experiments. C.B. and A.M. conceived, and C.B. and S.-Y.L. implemented the fluorescence microscopy-based tethering assays. T.G. did the electron microscopy. S.F. and M.V. developed the high-throughput Y2H technology, and R.P. and M.V. executed and interpreted Y2H screens and assays. S.-Y.L. and A.M. wrote the paper.

nucleotide exchange factors (GEFs) that catalyze GDP expulsion to allow GTP binding, and are inactivated by GTPase accelerating proteins (GAPs) that trigger the hydrolysis of GTP to GDP. Active GTP-bound Rabs recruit effector proteins that execute diverse functions including cytoskeletal transport, activation of lipid kinases, vesicle tethering, and SNARE-mediated fusion.

Abundant evidence indicates that many Rabs and Rab effectors promote membrane tethering. However, tethering activity has generally been inferred from *in vivo* experiments or from assays using cell extracts or organelles. In these complex reaction systems, hundreds or thousands of molecular species are present, with some directly mediating tethering while others act as upstream regulators that promote tethering but do not directly mediate it. For example, mammalian Rab5 regulates the homotypic tethering and fusion of endosomes[4–9]. Rab5 promotes phosphatidylinositol-3-kinase activity that in turn generates binding sites for other molecules that mediate tethering, including the Rab5 effector EEA1[10–12]. EEA1 binding to 3-phosphoinositides is essential for its tethering activity *in vivo*. However, mutations in EEA1 that abrogated its high-affinity interactions with Rab5 did not interfere with EEA1 membrane association or endosome tethering. Instead, these mutations acted downstream of tethering to block homotypic fusion[13]. Thus, while both Rab5 and EEA1 are unambiguously involved in endosome tethering, it remains uncertain whether Rab5 promotes tethering mainly by serving as a mechanical anchor for EEA1 (*i.e.*, Rab5 is part of the core tethering machinery), or whether the major role of Rab5 is to send instructive signals to other core tethering factors. There are similar uncertainties for the yeast Rab5 ortholog Vps21 and its effectors, and for the vast majority of other Rab-effector systems as well.

A central challenge in biochemistry is to reconstitute key biological processes using purified components, so as to define minimal reaction systems and explore their modes of action (*e.g.*, refs. 14,15,16,17). To date, only a handful of proteins have rigorously been shown to mediate tethering in chemically defined systems. These include GMAP-210, an effector of Arf1 at the Golgi[18], and HOPS, an effector of Ypt7 at the yeast vacuole[19–21]. For the vast majority of effectors currently known to promote tethering, it remains uncertain whether their modes of action are mechanical or regulatory. Thus, the development of quantitative approaches to dissect the activities of putative tethering factors, especially factors that interact with Rabs, is a major goal for the field. While developing a general set of methods for this purpose, we discovered that Vps21 and other endosomal Rab proteins in *Saccharomyces cerevisiae* not only bind classical effectors[22–27] but undergo GTP-regulated Rab-Rab interactions that directly drive tethering *in vitro*, in the complete absence of effectors. These findings reveal an unanticipated intrinsic activity of endosomal Rabs in *S. cerevisiae*, and imply the presence of an additional layer of membrane-membrane recognition events in endosomal membrane traffic.

Results

Vps21-GTP tethers in the absence of Rab effectors

To directly and quantitatively evaluate the tethering capabilities and mechanisms of Rabs and effectors, we developed liposome-based *in vitro* systems. Native Rab proteins generally

consist of a compact globular N-terminal GTP-binding domain, and a C-terminal intrinsically disordered hypervariable domain of ~30 residues. Rabs associate with membranes through two geranylgeranyl lipids which are covalently attached to the extreme C-terminus of the hypervariable domain. In our experiments, this lipid anchor was replaced by a C-terminal polyhistidine tag, which binds avidly to a synthetic lipid, Ni^{2+}-NTA-DOGS ((Ni^{2+}-1,2-diolyeoyl-*sn*-glycero-3-[(N(5-amino-1-carboxypentyl) iminodiacetic acid)succinyl]). Liposomes (~100 nm diameter) doped with Ni^{2+}-NTA-DOGS were prepared by extrusion, and the liposomes were then decorated with C-terminally His_{10}-tagged Rabs (Fig. 1a; see also ref. 28). Liposome tethering was measured by quasielastic light scattering (QLS), which reports tethering in real time as an increase in effective particle diameter. The response of the QLS system was validated using mixtures of extruded liposomes of different diameters (see Supplementary Methods).

Unexpectedly, we observed robust GTP-dependent increases in effective particle diameter when liposomes were decorated with the *Saccharomyces cerevisiae* endosomal Rab Vps21, in the absence of any additional effector proteins (Fig. 1b). This particle size increase was nearly eliminated when Vps21 was preloaded with GDP rather than GTP, or when liposomes were decorated with the vacuolar-lysosomal Rab Ypt7. Because the particle size increases reported by QLS might have been due to either liposome tethering or membrane fusion, we examined aliquots from the liposome preparations by negative stain transmission electron microscopy (TEM; Fig. 1c). TEM revealed massive clusters of Vps21- GTP-decorated liposomes, but no there was no evident size increase of individual liposomes within the clusters. Similarly, light microscopic observations of suspensions of fluorescently labeled liposomes in aqueous buffer (Fig. 1d) revealed thousands of visible clusters in the presence of Vps21-GTP. Importantly, after extended incubations, the diffuse fluorescent background of individual, fast-diffusing Vps21-GTP liposomes was markedly depleted, indicating that by 40 min of incubation most of the liposomes in the starting population had become tethered within large clusters. These observations indicate that the Vps21-GTP liposome clusters seen by TEM -formed in aqueous suspension, prior to deposition on the grid and negative staining. In sharp contrast to the tethering seen with Vps21-GTP, liposomes decorated with Vps21-GDP, or liposomes decorated with Ypt7 bound to either GDP or GTP (Figs 1c, d) did not form large clusters when examined by light or electron microscopy. Thus, three independent lines of evidence (QLS, TEM, and fluorescence microscopy) indicate that Vps21-GTP drives efficient Rab-selective and GTP-dependent liposome tethering *in vitro*.

Tethering occurs at physiological Rab surface densities

To further characterize Vps21-mediated tethering, we titrated Rabs and lipids (Figs. 2a, 2b and Supplementary Fig. 1). The Ni^{2+} chelator lipid NTA-DOGS is anionic. The nitrilotriacetic acid (NTA) moiety has a net charge of −3, and binds Ni^{2+} with 1:1 stoichiometry[29]. Ni^{2+}-NTA-DOGS-doped liposomes, like endocytic organelles, therefore have a net negative charge. Over a range of Ni^{2+}-NTA-DOGS concentrations, strong tethering signals were observed at His_{10}-Vps21 surface densities of 1500–7000 $\cdot \mu m^{-2}$. In a comparable *in* vitro reconstitution of liposome tethering by another small G protein, Arf1, and its effector GMAP, tethering was observed at Arf1 densities of 8000–14000 $\cdot \mu m^{-2}$ and

GMAP densities of 700–7000 · μm^{-2} (ref. 18). Notably, we found that tethering was sharply responsive to the Vps21-GTP surface density (Supplementary Fig. 1a; Hill coefficient ≥3.5, 95% confidence limit). A simple interpretation of this dosage hypersensitivity is that tethering occurs through a cooperative mechanism that entails the concerted action of several Vps21-GTP complexes. Tethering was dramatically reduced when liposomes were decorated with inactive Vps21-GDP (Figs 2a, 2b and S1b). At very high ratios of Vps21-His_{10} to Ni^{2+}-NTA-DOGS tethering was inhibited, probably through competitive inhibition by unbound Vps21-His_{10} (Supplementary Fig. 1b). With the vacuolar Rab Ypt7 (Supplementary Fig. 1c), tethering was never observed at any concentration of Ni^{2+}-NTA-DOGS or Ypt7. This result is consistent with the demonstrated requirement for the HOPS effector complex in Ypt7-mediated tethering[19–21] and underscores the selectivity of Vps21-mediated tethering.

We next sought to determine whether Vps21-mediated tethering occurs within a physiologically relevant span of surface densities. To provide a criterion for the onset of tethering, we defined the critical surface density for tethering as the density of surface-bound Rab at which the effective particle diameter, measured by QLS, increases to twice the effective diameter of bare, untethered control liposomes. Nominally, at the critical surface density each liposome is on average tethered to one other liposome. The critical surface density for tethering by Vps21-GTP was ≤1300 μm^{-2} (Figs. 2a and 2b, insets). This density corresponds to ~40 Vps21 molecules on the surface of a 100 nm diameter endosome, or ~10 molecules on a 50 nm endosome. Note that these are upper-bound estimates which assume that every Vps21 molecule in the assay system is both active and bound to a liposome. Although the Vps21 surface density on endosomes *in vivo* is unknown, estimates are available for the surface densities of two other Rabs. The density of Ypt7 on the *S. cerevisiae* vacuole is ~500 μm^{-2}, and the density of Rab3a on mammalian synaptic vesicles is ~1,950 μm^{-2} (Supplementary Methods; refs. 30–32). GTP-regulated tethering by Vps21 therefore occurs within the physiologically relevant range of Rab surface densities. Below this range detectable tethering does not occur, while above this range regulation by GTP binding is attenuated and tethering occurs constitutively.

To further characterize the interactions that drive Vps21-mediated tethering, we performed QLS-based tethering assays across a range of salt concentrations (Fig. 2c, d). At sub-physiological ionic strengths, tethering was potently inhibited. As the buffer ionic strength increased, the efficiency of tethering increased and then leveled off. Under all ionic conditions tested, GTP selectivity was observed, but the highest selectivity was at physiological ionic strength (150–200 mM NaCl). Inefficient tethering at low ionic strength could result from reduced shielding of the electrostatic repulsion between the negatively-charged liposomes, or from decreased hydrophobic forces at protein interaction surfaces.

Rab-Rab interactions in trans drive efficient tethering

In principle, Vps21-mediated tethering might occur through either a symmetric or an asymmetric mechanism (Fig. 3a). In the symmetric mechanism, Vps21 anchored to opposite membranes would dimerize or oligomerize *in trans* to drive tethering. This mechanism depends on protein-protein contacts. In the asymmetric mechanism, a single Vps21 molecule

anchored to one vesicle would undergo GTP-triggered direct binding to the lipids of the opposite vesicle. It is also possible that both classes of mechanisms could contribute to Vps21-mediated tethering.

To assess these hypotheses, we employed a bead-liposome assay that allows the components on two tethering surfaces to be varied independently (Fig. 3b). A similar system was previously used to probe the binding of nucleoporin proteins to phospholipid bilayers[33]. Large (~100 μm) glutathione-agarose beads were decorated with glutathione-*S*-transferase (GST)-Rab fusion proteins. The beads were mixed with a suspension of small (~100 nm) fluorescent liposomes with Rab-His_{10} proteins. Tethering of the liposomes to the beads was evident by epifluorescence microscopy as a fluorescent halo at the bead's surface (Fig. 3c). Using this assay we found that efficient tethering requires GTP-bound Vps21 anchored to both partner surfaces. Tethering did not occur when Vps21-His_{10} was absent (Fig. 3d) or when Vps21-His_{10} attachment to liposomes was prevented by omission of Ni^{2+}-NTA-DOGS (Fig. 3e). Similarly, tethered liposomes fell off of the beads when GST-Vps21 was dissociated from the beads by soluble glutathione (Fig. 3f). Tethering was also abrogated when Ypt7 replaced Vps21 on either the beads or the liposomes (Supplementary Fig. 2a). The inability of bead-bound GST-Vps21 to tether either bare liposomes or liposomes bearing Ypt7 is evidence against asymmetric tethering mechanisms in which GTP-binding triggers a Vps21 interaction solely by interacting with the *trans* bilayer. Moreover, substitution of GDP for GTP on GST-Vps21 (beads), on Vps21-His_{10} (liposomes), or both substantially attenuated tethering (Supplementary Fig. 2b). Thus for optimal tethering, Rabs on both partner surfaces must be activated. This result mirrors the symmetrical requirement for activated Rab5-GTP in homotypic docking and fusion of mammalian endosomes[9]. In sum, these results support models in which symmetrical Vps21-Vps21 contacts *in trans* are required for tethering. We note, however, that we have so far been unable to detect Vps21 dimerization or oligomerization in solution-based assays (e.g., Supplementary Fig. 3). Together, these results suggest that restraining Vps21 on a two-dimensional membrane surface may increase avidity to drive tethering. It is also possible, however, that affinity components derived from both protein-membrane and protein-protein interactions are required for efficient tethering (see Discussion).

The Vps21 C-terminal linker is not required for tethering

Native Vps21, like most other Rabs, consists of a compact N-terminal GTP-binding domain that attaches to membranes through a disordered ~30-residue C-terminal linker bearing a doubly geranylgeranylated membrane anchor at its extreme C-terminus. To ascertain whether the Vps21 C-terminal linker contributes to tethering, we prepared a set of Vps21-His_{10} mutants with truncated C-terminal linkers (Fig. 4a), and evaluated the capacity of these mutants to promote liposome tethering in the QLS assay (Fig. 4b). Each of the mutants mediated GTP-dependent tethering with efficiency equivalent to or greater than that of full-length Vps21. Thus, the C-terminal linker domain is not directly involved in the tethering reaction.

Vps21 interacts with other endosomal Rabs to drive tethering

Taken together, our biochemical studies suggest that efficient Vps21-mediated tethering involves a protein-protein interaction: GTP-stimulated Vps21–Vps21 association *in trans*. Unbiased yeast two-hybrid (Y2H) screens provided additional corroborating evidence that Vps21 interacts with itself and also with other endosomal Rabs.

In a separate project, we sought to identify new Rab-interacting proteins by performing systematic Y2H screens. In all of our Y2H experiments, we used low-copy rather than high-copy vectors, and the read-out growth assays were always performed in the presence of 3-aminotriazole, conditions that almost eliminate false positives[34,35]. Using the eleven *S. cerevisiae* Rabs as baits, we interrogated ordered prey arrays containing over 5000 *S. cerevisiae* open reading frames. More than 65,000 crosses yielded ~340 candidate interactions. Among these interactions were numerous expected Rab interactions with known Rab effectors (Ref. 36 and unpublished results), as well as expected interactions with Rab-specific chaperones including Rab GDI (GDP dissociation inhibitor), Rab escort protein, and Yif and Yip proteins (Supplementary Table 1). Unexpectedly, however, the screen repeatedly identified homotypic and heterotypic Rab-Rab interactions among endosomal Rabs. In our initial screens the Rab5 orthologs Vps21, Ypt52, Ypt53, and Ypt10, the Rab6 ortholog Ypt6, and the Rab 7 ortholog Ypt7 were detected in heterotypic and homotypic Rab-Rab interactions (Supplementary Table 1). Moreover, physical interactions among Vps21, Ypt52, and Ypt53 were independently reported in high-throughput proteomic surveys[37], and mammalian Rab5 isoforms were independently reported to undergo GTP-dependent dimerization[38].

In focused Y2H assays using independently constructed prey vectors, most of the interactions detected in the high-throughput screens were reproduced and extended (Table S2), with the Vps21 self-interaction yielding an especially robust signal (Fig. 5; Supplementary Tables 2 and 3). Importantly, Vps21 interactions with itself and with other Rabs were restricted to wild type Vps21 and the dominant-active mutant $Vps21_{Q66L}$. Moreover, these Y2H interactions were similar in signal strength and nucleotide selectivity to Vps21 interactions with its three known effectors: Vps3, Vps8, and Vac1[22,23,27,39]. Neither Rab-Rab nor Rab-effector interactions were observed when either bait or prey was the GDP-biased mutant $Vps21_{S21L}$. As expected, the $Vps21_{S21L}$ mutant robustly interacted with the Vps21 nucleotide exchange factor Vps9 (ref. 40) but not with Vps21 effector proteins. These Y2H data provide evidence for GTP-dependent interactions among multiple yeast endosomal Rab proteins and buttress our biochemical results showing that Vps21-mediated tethering is driven by homotypic interactions between activated, membrane-anchored Vps21 molecules.

To ascertain whether heterotypic interactions between Vps21 and other Rabs can drive tethering, as suggested by the Y2H results, we employed the bead-liposome assay (Fig. 6). Beads decorated with various GST-Rab fusions were mixed with fluorescent liposomes bearing $Vps21\text{-}His_{10}$. In these assays (Fig. 6a), tethering was mediated by Vps21-GTP with Ypt53 or Ypt10, two other Rabs of the endosomal Rab5 group[41]. In each case, substitution of GDP for GTP abrogated tethering (Fig. 6b). Several other Rabs including another Rab5

paralog, Ypt52, did not mediate heterotypic tethering with Vps21 (Figs. 6a). We note that since Vps21-GTP liposomes can interact with one another, there may be competition between Vps21 on the liposomes and the Rabs displayed on the beads, reducing the apparent heterotypic tethering signal between Vps21 and any Rabs that Vps21 binds with lower affinity than the self-interaction. This type of competition, if it did occur, would make the bead-liposome assay more stringent, and could prevent detection of weaker Rab-Rab tethers. Taken together, the Y2H experiments and tethering assays reveal a network of GTP-stimulated homotypic and heterotypic interactions among endosomal Rabs. A subset of these pairs is able to mediate GTP-dependent tethering *in vitro*.

Regulation of tethering by Vps21GEF and GAP

Regulation and reversibility are hallmarks of Rab-controlled tethering reactions. Upstream regulators of Vps21 include Vps9, a GEF[40], and Gyp1, a GAP[42,43]. We therefore evaluated whether Vps9 and $Gyp1_{TBC}$ (the Gyp1 catalytic core) can control Vps21-mediated tethering. Using solution-phase assays, we first verified the catalytic activities of our Vps9 and $Gyp1_{TBC}$ preparations (Supplementary Fig. 4). We then asked whether Vps9 could stimulate tethering by promoting nucleotide exchange. Liposomes bearing Vps21-GDP, monitored by QLS, tethered when both GTP and Vps9 were added to the reactions (Fig. 7a). Next, we examined the reversibility of tethering. When added to pre-tethered liposomes bearing Vps21-GTP, the GAP $Gyp1_{TBC}$ efficiently reversed tethering, again with dose-dependent kinetics at concentrations as low as 10 nM (Fig. 7b). The catalytically inactive mutant[43] $Gyp1_{TBC\text{-}R343K}$ had no effect on tethering even when added at 10 μM. GTP hydrolysis is therefore essential for the $Gyp1_{TBC}$-mediated disassembly of Vps21-GTP-mediated tethers (Fig. 7b).

Finally, in sequential-addition experiments, we were able to reconstitute a complete cycle of regulated tethering and de-tethering (Fig. 7c–e). Liposomes decorated with Vps21-GDP were monitored by QLS (Fig. 7c). Addition of GTP alone had no effect, but subsequent Vps9 addition initiated an immediate and steady increase in tethering. Addition of $Gyp1_{TBC}$ rapidly reversed Vps9-stimulated tethering. QLS-derived particle size distributions (Fig. 7d), and TEM analysis of aliquots taken from the same reactions (Fig. 7e) verified that Vps9 and $Gyp1_{TBC}$ can drive complete cycles of tethering and de-tethering. Thus, Vps21-mediated tethering in the absence of effectors is Rab-selective, GTP-regulated, completely reversible, and strictly controlled by upstream regulators.

Discussion

Small G-proteins orchestrate a multitude of biological processes, generally by acting through specialized effectors. Nevertheless, some small G-proteins have intrinsic capabilities that complement or enhance the activities of their effectors. In vesicle formation, for example, activated Arf1 and Sar1 recruit the COPI and COPII coat complexes. However, the N-terminal domains of these small G-proteins also interact directly with membranes to generate positive membrane curvature[44,45]. Here, we have shown that similar to Arf1 and Sar1, Vps21 and some other yeast endosomal Rab proteins have intrinsic as well as effector-mediated capabilities: they can dimerize or oligomerize *in trans* to tether membranes in a

stringently GTP-dependent, tightly regulated, and fully reversible reaction. In our working model this intrinsic tethering mechanism would cooperate with classical Rab-effector mechanisms to promote membrane tethering, docking, and fusion (Fig. 8).

There are previous reports of Rab-Rab interactions. Rab5a, Rab5b, and Rab5c, the closest mammalian orthologs of Vps21, were detected in homotypic and heterotypic dimers by Y2H, and Rab5b was shown to dimerize *in vitro* and *in vivo* in an apparently GTP-dependent manner[38]. Moreover, in structural studies the GDP-bound forms of Rab9 and Rab11a were reported to form crystallographic dimers[46–48]. To date, all Rabs reported to dimerize operate within endocytic trafficking pathways. These interactions are consistent with our results for yeast endocytic Rabs, raising the possibility that dimerization of endocytic Rabs is a more general theme. The potential for complex regulation of tethering through Rab-Rab interactions is underscored by our identification of Rab pairs that exhibit heterotypic interactions in Y2H experiments, and by our demonstration that a subset of these Rab pairs mediates heterotypic tethering in the liposome-bead assay. Similarly Arf1, another small G-protein, was reported to dimerize during vesicle formation[49]. However, Arf1 did not mediate membrane tethering except in the presence of an effector[18]. Dimerization of Arf1 therefore appears to be restricted to *cis* rather than *trans* interactions.

Our biochemical and biophysical results demonstrate that Vps21 and some other endosomal Rabs have an intrinsic ability to tether membranes *in vitro*. Nevertheless, important questions about the detailed mechanism of this tethering activity and its biological consequences remain to be answered. While our results strongly indicate that Vps21-Vps21 interactions are involved in tethering, we have so far been unable to detect Vps21 dimerization or oligomerization in solution phase assays using techniques including size exclusion chromatography and multiangle light scattering. These findings raise the possibility that Vps21 dimerization is augmented by as yet uncharacterized interactions between Vps21-GTP and the membrane. A requirement for both protein-protein interactions and protein-membrane interactions in GTP-triggered tethering would be reminiscent of the requirement for interactions between synaptotagmin and SNARE proteins, as well as between synaptotagmin and lipids, in Ca^{2+}-triggered fusion[50].

The relative *in vivo* contributions to yeast endosome tethering by intrinsic Vps21 activity and by more conventional Vps21-effector mechanisms are not yet characterized, and remain to be dissected *in vivo*. Such experiments will require the isolation of Vps21 mutants that interact with the normal complement of Rab chaperones, upstream regulators, and effectors, but which lack intrinsic tethering capacity. We are currently performing genetic screens to identify and characterize mutant alleles with these properties.

If Rabs recruit specialized effectors, some of which are tethers, what is the function of Rab-Rab tethering? We suggest two possibilities. First, it is quite clear that there is some redundancy among Rabs and effectors. For example, the yeast protein Vps8 is the only effector of Vps21 currently known to promote tethering *in vivo*. Vps8 is also needed for biosynthetic trafficking of carboxypeptidase Y (CPY) to the vacuole. Importantly, however, functional defects caused by Vps8 deletion were efficiently suppressed by Vps21 overproduction[24]. Conversely, Vps8 overexpression in the absence of Vps21 does not

appear to mediate tethering[26]. These results support working models in whichVps8 and Vps 21 normally act in concert, while in the absence of Vps8, an elevated level of secondary Vps21-mediated tethering is sufficient to support endolysosomal traffic. This secondary tethering activity could be mediated by Vps21-Vps21 interactions, by Vps21 interactions with another effector, or by some combination of these activities.

A second possible function for Rab-Rab tethering is suggested by the fact that Rab-Rab tethers almost certainly operate at shorter range than classical effector-based tethers. Known and presumed tethers often assume extended structures that are presumed to allow vesicle capture and tethering over substantial distances (tens of nm). In contrast, Rab-Rab tethering must occur over shorter distances. Most Rabs attach to the membrane through a ~35 residue C-terminal disordered linker, doubly prenylated at its end. Our results show that the Vps21 linker is not needed for tethering (Fig. 4), but it probably influences the distance between tethered membranes. Because disordered polypeptides act as Brownian springs, it is likely that Rabs interact *in trans* between membranes separated by ≤10 nm (Fig. 8; Supplementary Methods). Similarly, kinetically stable *trans*-SNARE complexes assemble only once docked membranes approach to within ~8 nm[51,52], raising the possibility of a “handoff” mechanism whereby effector-mediated tethers promote Rab-Rab tethering, which in turn stably hold the membranes close enough promote the initiation of SNARE zippering and fusion (Fig. 8). In the cases of Rab5 and Vps21, SNARE pairing is regulated by Vps45, an SM-family protein recruited to the fusion site by Rab5 effector Rabenosyn-5 or its yeast ortholog Vac1[22,23,53,54]. Finally, we speculate that Rab-Rab tethering might have emerged early in eukaryotic evolution, preceding more complex systems in which effectors brought to bear additional capabilities: coordination of multiple small G-proteins[2,55], tethering over longer distances[56], coupling of Rab activation to vesicle coat dynamics[57], and *trans*-SNARE complex assembly and membrane fusion[21,52,58].

ONLINE METHODS

Proteins

See Supplementary Methods for detailed descriptions of protein expression construct, expression, and purification.

Liposomes

Egg PC and Ni^{2+}-NTA-DOGS dissolved in chloroform (Avanti Polar Lipids) were mixed, dried under an argon stream, and placed under vacuum overnight. For assays requiring fluorescent liposomes, 0.4 mol% Texas Red DPPE (Invitrogen) was incorporated into the lipid mixture. Lipid films were hydrated in liposome reaction buffer (20 mM HEPES · NaOH, pH 7.5, 150 mM NaCl, 1 mM $MgCl_2$, and 2 mM 2-mercaptoethanol) to 2.5 mg ml^{-1} before extrusion through a 0.1 μm polycarbonate filter (Avanti Polar Lipids). To change the ionic strength of the liposome environment, liposomes were prepared in liposome reaction buffer at the indicated NaCl concentrations.

QLS tethering assay

In general, samples were prepared by incubating 100 μl of liposomes with 20 μl of nucleotide-loaded Rab-His_{10} at RT for 1 hour, then diluted to 1 ml for QLS measurement. See Supplementary Methods for detailed information on QLS. Nucleotide-loaded Rab-His_{10} protein was prepared by incubating 4–5 mg ml^{-1} of Rab-His_{10} with a 30-fold molar excess of guanine nucleotide and 5 mM EDTA for 1 hour at 25–27°C in 20 mM HEPES · NaOH, pH 7.5, 150 mM NaCl, and 1 mM dithiothreitol. Nucleotide exchange was terminated with 10 mM $MgCl_2$ on ice for 15 min and free nucleotide was removed by size exclusion using a Micro Bio-Spin column (Bio-Rad) pre-equilibrated with liposome reaction buffer at the indicated NaCl concentration.

Rab membrane density was altered by incubating liposomes at varying Rab to Ni^{2+}-NTA-DOGS molar ratios (Supplementary Table 4). Except as indicated, liposomes contained 4.5 mol% Ni^{2+}-NTA-DOGS and were incubated with 20 μl of Rab-His_{10} at 0.067 Rab to Ni^{2+}-NTA-DOGS molar ratio, ≤3750 Vps21-His_{10} per $μm^2$. For GEF experiments, Vps9 was added to 200 μl of liposomes pre-incubated with GDP-bound Vps21-His_{10} and diluted to 640 μl for QLS measurement. 10 μl GTP was added to initiate tethering. For GAP experiments, 200 μl of liposomes pre-incubated with GTP-loaded Vps21-His_{10} was diluted to 550 μl for QLS measurement. 100 μl of $Gyp1_{TBC}$ or $Gyp1_{TBC\text{-}R343K}$ was added to initiate disassembly of liposome clusters. For the reconstitution of a full tethering cycle, 400 μl of liposomes were pre-incubated with GDP-bound Vps21-His_{10}. The mixture was diluted to 640 μl for QLS measurements, and GTP, Vps9, and $Gyp1_{TBC}$ were subsequently added, in order, to final volumes of 650 μl, 700 μl, and 850 μl. The concentrations of GTP, Vps9 and $Gyp1_{TBC}$ were maintained at 20 μM, 5 μM, and 10 μM, respectively, throughout the sequential-addition experiment.

Fluorescent tethering assay and bead-liposome tethering assay

GST-Rab coupled glutathione–Sepharose 4B beads (GE Healthcare) were prepared as described[27,36] except that an equal volume of *E. coli* lysate expressing untagged $Gyp1_{TBC}$ was mixed with the Rab-expressing cell lysate to drive Rab conversion into the GDP-bound state. Nucleotide loading of Rabs was performed by incubating GST-Rab beads in loading buffer (50 mM HEPES · NaOH (pH 7.8), 100 mM NaCl, 5 mM 2-mercaptoethanol, 5 mM EDTA, and 500 μM guanine nucleotide) for 1 hour at room temperature. An equal volume of quenching buffer (50 mM HEPES · NaOH, pH 7.8, 100 mM NaCl, 5 mM 2-mercaptoethanol, and 10 mM $MgCl_2$) was then added to each reaction and incubated for an additional 15 min. Nucleotide-loaded GST-Rab beads were then washed twice with reaction buffer (20 mM HEPES · NaOH, pH 7.4, 125 mM NaCl, 5 mM 2-mercaptoethanol, and 5 mM $MgCl_2$). Fluorescent liposome tethering reactions or bead-liposome tethering reactions were prepared on ice by mixing 50 μl reaction buffer and 40 μl of fluorescent liposome suspension in the absence or presence of 50 μl of packed, nucleotide-loaded GST-Rab beads. 6 μg of nucleotide-loaded Rab-His_{10} was then added to initiate tethering. The upper-bound density of Vps21-His_{10} on liposomes used for the bead assay was ≤4700 Vps21-His_{10} per $μm^2$. Reactions were brought to room temperature, incubated for 20, 40, or 60 min, and imaged.

Micrographs were acquired using a microscope (IX71; Olympus) equipped with an electron-multiplying charge-coupled device (iXon; Andor). Epifluorescence illumination was by green and blue light-emitting diodes (>350-mW output) coupled to the microscope's back aperture by a multimode optical fiber and driven by custom electronics. Objective lenses were UPlanApo 0.40 NA 10 × or PlanApoN 1.45 NA 60 ×. The microscope and camera were driven by iQ software (version 6.0.3.62; Andor), and micrographs were processed using ImageJ (version 1.36b; National Institutes of Health) and Photoshop (version 8.0; Adobe). For display, images were sharpened by applying unsharp masking.

Electron microscopy

For negative stain electron microscopy samples were stained with 0.75% (m/v) uranyl formate. Images were collected using a 100 kV transmission electron microscope (Morgagni M268, FEI) equipped with at Gatan bottom mount 4k × 2k charge coupled device (CCD) camera. Images were recorded at either 4400 × or 8900 × magnification at the specimen level.

Yeast two-hybrid

Genome-wide two-hybrid analysis was performed as previously reported[13] in collaboration with the University of Washington Yeast Resource Center. Parent strains and plasmids were obtained from the Yeast Resource Center. Two-hybrid constructs were cloned individually into haploid tester strains using gap-repair and homologous recombination. Prey domains were cloned into the plasmid pOAD and transformed into the yeast strain PJ69-4a. Bait domains were cloned into pOBD2 and transformed into PJ69-4α. Clonal isolates were obtained and verified by PCR. Sequencing was done using dideoxy chain termination.

Focused interaction tests were performed by mating bait and prey haploid strains in 96-well plates which were then pinned to YPD plates supplemented with adenine using a 48-spoke inoculating manifold. The mating plates were grown at 30° C overnight before selecting diploids by replica plating onto medium supplemented with adenine but lacking tryptophan and leucine. Diploid colonies were grown at 30° C for two days, then replica plated to medium supplemented with adenine and 1.5 mM 3-amino-1,2,4-triazole (3-AT) but lacking tryptophan, leucine, and histidine. Plates were scored for growth after 5 days at 30° C.

Supplementary Material

Refer to Web version on PubMed Central for supplementary material.

Acknowledgments

We thank P. Brennwald and J. Taraska for helpful discussion, and D. Baker and R. Koga for assistance with multiangle light scattering experiments. High-throughput screening was done through the Yeast Resource Center (National Institutes of Health P41 RR11823). S.L. was supported in part by University of Washington Nanotechnology Integrative Graduate Education and Research Traineeship award (National Science Foundation DGE-0504573). We thank the Murdock Charitable Trust and the Washington research Foundation for generous support of our electron cryomicroscopy laboratory. T.G. was a Howard Hughes Medical Institute Early Career Scientist. This work was supported by National Institutes of Health grant GM077349 and Research Scholar Grant 10-026-01-CSM from the American Cancer Society.

References

1. Kornmann B, et al. An ER-mitochondria tethering complex revealed by a synthetic biology screen. Science. 2009; 325:477–481. [PubMed: 19556461]
2. Grosshans BL, Ortiz D, Novick P. Rabs and their effectors: achieving specificity in membrane traffic. Proc Natl Acad Sci U S A. 2006; 103:11821–11827. [PubMed: 16882731]
3. Barr FA. Rab GTPase function in Golgi trafficking. Semin Cell Dev Biol. 2009; 20:780–783. [PubMed: 19508857]
4. Singer-Kruger B, et al. Role of three Rab5-like GTPases, Ypt51p, Ypt52p, and Ypt53p, in the endocytic and vacuolar protein sorting pathways of yeast. J Cell Biol. 1994; 125:283–298. [PubMed: 8163546]
5. Horazdovsky BF, Busch GR, Emr SD. *VPS21* encodes a Rab5-like GTP binding protein that is required for the sorting of yeast vacuolar proteins. EMBO J. 1994; 13:1297–1309. [PubMed: 8137814]
6. Gerrard SR, Bryant NJ, Stevens TH. *VPS21* controls entry of endocytosed and biosynthetic proteins into the yeast prevacuolar compartment. Mol Biol Cell. 2000; 11:613–626. [PubMed: 10679018]
7. Gorvel JP, Chavrier P, Zerial M, Gruenberg J. Rab5 controls early endosome fusion in vitro. Cell. 1991; 64:915–925. [PubMed: 1900457]
8. Bucci C, et al. Co-operative regulation of endocytosis by three Rab5 isoforms. FEBS Lett. 1995; 366:65–71. [PubMed: 7789520]
9. Barbieri MA, et al. Evidence for a symmetrical requirement for Rab5-GTP in in vitro endosome-endosome fusion. J Biol Chem. 1998; 273:25850–25855. [PubMed: 9748259]
10. Simonsen A, et al. EEA1 links PI(3)K function to Rab5 regulation of endosome fusion. Nature. 1998; 394:494–498. [PubMed: 9697774]
11. Christoforidis S, McBride HM, Burgoyne RD, Zerial M. The Rab5 effector EEA1 is a core component of endosome docking. Nature. 1999; 397:621–625. [PubMed: 10050856]
12. Christoforidis S, et al. Phosphatidylinositol-3-OH kinases are Rab5 effectors. Nat Cell Biol. 1999; 1:249–252. [PubMed: 10559924]
13. Lawe DC, et al. Sequential roles for phosphatidylinositol 3-phosphate and Rab5 in tethering and fusion of early endosomes via their interaction with EEA1. J Biol Chem. 2002; 277:8611–8617. [PubMed: 11602609]
14. Davie EW. A brief historical review of the waterfall/cascade of blood coagulation. J Biol Chem. 2003; 278:50819–50832. [PubMed: 14570883]
15. Weber T, et al. SNAREpins: minimal machinery for membrane fusion. Cell. 1998; 92:759–772. [PubMed: 9529252]
16. Antonny B, Madden D, Hamamoto S, Orci L, Schekman R. Dynamics of the COPII coat with GTP and stable analogues. Nat Cell Biol. 2001; 3:531–537. [PubMed: 11389436]
17. Wollert T, Hurley JH. Molecular mechanism of multivesicular body biogenesis by ESCRT complexes. Nature. 2010; 464:864–869. [PubMed: 20305637]
18. Drin G, Morello V, Casella JF, Gounon P, Antonny B. Asymmetric tethering of flat and curved lipid membranes by a golgin. Science. 2008; 320:670–673. [PubMed: 18451304]
19. Hickey CM, Wickner W. HOPS Initiates Vacuole Docking by Tethering Membranes Prior to trans-SNARE Complex Assembly. Mol Biol Cell. 2010
20. Hickey CM, Stroupe C, Wickner W. The major role of the Rab Ypt7p in vacuole fusion is supporting HOPS membrane association. J Biol Chem. 2009; 284:16118–16125. [PubMed: 19386605]
21. Stroupe C, Hickey CM, Mima J, Burfeind AS, Wickner W. Minimal membrane docking requirements revealed by reconstitution of Rab GTPase-dependent membrane fusion from purified components. Proc Natl Acad Sci U S A. 2009; 106:17626–17633. [PubMed: 19826089]
22. Peterson MR, Burd CG, Emr SD. Vac1p coordinates Rab and phosphatidylinositol 3-kinase signaling in Vps45p-dependent vesicle docking/fusion at the endosome. Curr Biol. 1999; 9:159–162. [PubMed: 10021387]

23. Tall GG, Hama H, DeWald DB, Horazdovsky BF. The phosphatidylinositol 3-phosphate binding protein Vac1p interacts with a Rab GTPase and a Sec1p homologue to facilitate vesicle-mediated vacuolar protein sorting. Mol Biol Cell. 1999; 10:1873–1889. [PubMed: 10359603]
24. Horazdovsky BF, Cowles CR, Mustol P, Holmes M, Emr SD. A novel RING finger protein, Vps8p, functionally interacts with the small GTPase, Vps21p, to facilitate soluble vacuolar protein localization. J Biol Chem. 1996; 271:33607–33615. [PubMed: 8969229]
25. Peplowska K, Markgraf DF, Ostrowicz CW, Bange G, Ungermann C. The CORVET tethering complex interacts with the yeast Rab5 homolog Vps21 and is involved in endo-lysosomal biogenesis. Dev Cell. 2007; 12:739–750. [PubMed: 17488625]
26. Markgraf DF, et al. The CORVET subunit Vps8 cooperates with the Rab5 homolog Vps21 to induce clustering of late endosomal compartments. Mol Biol Cell. 2009; 20:5276–5289. [PubMed: 19828734]
27. Plemel RL, et al. Subunit organization and Rab interactions of Vps-C protein complexes that control endolysosomal membrane traffic. Mol Biol Cell. 2011; 22:1353–1363. [PubMed: 21325627]
28. Gureasko J, et al. Membrane-dependent signal integration by the Ras activator Son of sevenless. Nat Struct Mol Biol. 2008; 15:452–461. [PubMed: 18454158]
29. Hochuli E, Dobeli H, Schacher A. New metal chelate adsorbent selective for proteins and peptides containing neighbouring histidine residues. J Chromatogr. 1987; 411:177–184. [PubMed: 3443622]
30. Wang L, Seeley ES, Wickner W, Merz AJ. Vacuole fusion at a ring of vertex docking sites leaves membrane fragments within the organelle. Cell. 2002; 108:357–369. [PubMed: 11853670]
31. Ghaemmaghami S, et al. Global analysis of protein expression in yeast. Nature. 2003; 425:737–741. [PubMed: 14562106]
32. Takamori S, et al. Molecular anatomy of a trafficking organelle. Cell. 2006; 127:831–846. [PubMed: 17110340]
33. Patel SS, Rexach MF. Discovering novel interactions at the nuclear pore complex using bead halo: a rapid method for detecting molecular interactions of high and low affinity at equilibrium. Mol Cell Proteomics. 2008; 7:121–131. [PubMed: 17897934]
34. Braun P, et al. An experimentally derived confidence score for binary protein-protein interactions. Nat Methods. 2009; 6:91–97. [PubMed: 19060903]
35. Chen YC, Rajagopala SV, Stellberger T, Uetz P. Exhaustive benchmarking of the yeast two-hybrid system. Nat Methods. 2010; 7:667–8. author reply 668. [PubMed: 20805792]
36. Brett CL, et al. Efficient termination of vacuolar Rab GTPase signaling requires coordinated action by a GAP and a protein kinase. J Cell Biol. 2008; 182:1141–1151. [PubMed: 18809726]
37. Ho Y, et al. Systematic identification of protein complexes in Saccharomyces cerevisiae by mass spectrometry. Nature. 2002; 415:180–183. [PubMed: 11805837]
38. Daitoku H, Isida J, Fujiwara K, Nakajima T, Fukamizu A. Dimerization of small GTPase Rab5. Int J Mol Med. 2001; 8:397–404. [PubMed: 11562778]
39. Pawelec A, Arsic J, Kolling R. Mapping of Vps21 and HOPS binding sites in Vps8 and effect of binding site mutants on endocytic trafficking. Eukaryot Cell. 2010
40. Hama H, Tall GG, Horazdovsky BF. Vps9p is a guanine nucleotide exchange factor involved in vesicle-mediated vacuolar protein transport. J Biol Chem. 1999; 274:15284–15291. [PubMed: 10329739]
41. Buvelot Frei S, et al. Bioinformatic and comparative localization of Rab proteins reveals functional insights into the uncharacterized GTPases Ypt10p and Ypt11p. Mol Cell Biol. 2006; 26:7299–7317. [PubMed: 16980630]
42. Du LL, Collins RN, Novick PJ. Identification of a Sec4p GTPase-activating protein (GAP) as a novel member of a Rab GAP family. J Biol Chem. 1998; 273:3253–3256. [PubMed: 9452439]
43. Pan X, Eathiraj S, Munson M, Lambright DG. TBC-domain GAPs for Rab GTPases accelerate GTP hydrolysis by a dual-finger mechanism. Nature. 2006; 442:303–306. [PubMed: 16855591]
44. Lee MC, et al. Sar1p N-terminal helix initiates membrane curvature and completes the fission of a COPII vesicle. Cell. 2005; 122:605–617. [PubMed: 16122427]

45. Pucadyil TJ, Schmid SL. Conserved functions of membrane active GTPases in coated vesicle formation. Science. 2009; 325:1217–1220. [PubMed: 19729648]
46. Wittmann JG, Rudolph MG. Crystal structure of Rab9 complexed to GDP reveals a dimer with an active conformation of switch II. FEBS Lett. 2004; 568:23–29. [PubMed: 15196914]
47. Pasqualato S, et al. The structural GDP/GTP cycle of Rab11 reveals a novel interface involved in the dynamics of recycling endosomes. J Biol Chem. 2004; 279:11480–11488. [PubMed: 14699104]
48. Scapin SM, et al. The crystal structure of the small GTPase Rab11b reveals critical differences relative to the Rab11a isoform. J Struct Biol. 2006; 154:260–268. [PubMed: 16545962]
49. Beck R, et al. Membrane curvature induced by Arf1-GTP is essential for vesicle formation. Proc Natl Acad Sci U S A. 2008; 105:11731–11736. [PubMed: 18689681]
50. Chapman ER. How Does Synaptotagmin Trigger Neurotransmitter Release? Annu Rev Biochem. 2008
51. Li F, et al. Energetics and dynamics of SNAREpin folding across lipid bilayers. Nat Struct Mol Biol. 2007; 14:890–896. [PubMed: 17906638]
52. Schwartz ML, Merz AJ. Capture and release of partially zipped trans-SNARE complexes on intact organelles. J Cell Biol. 2009; 185:535–549. [PubMed: 19414611]
53. Nielsen E, et al. Rabenosyn-5, a novel Rab5 effector, is complexed with hVPS45 and recruited to endosomes through a FYVE finger domain. J Cell Biol. 2000; 151:601–612. [PubMed: 11062261]
54. Furgason ML, et al. The N-terminal peptide of the syntaxin Tlg2p modulates binding of its closed conformation to Vps45p. Proc Natl Acad Sci U S A. 2009; 106:14303–14308. [PubMed: 19667197]
55. Sinka R, Gillingham AK, Kondylis V, Munro S. Golgi coiled-coil proteins contain multiple binding sites for Rab family G proteins. J Cell Biol. 2008; 183:607–615. [PubMed: 19001129]
56. Hayes GL, et al. Multiple Rab GTPase binding sites in GCC185 suggest a model for vesicle tethering at the trans-Golgi. Mol Biol Cell. 2009; 20:209–217. [PubMed: 18946081]
57. Angers CG, Merz AJ. New links between vesicle coats and Rab-mediated vesicle targeting. Semin Cell Dev Biol. 2011; 22:18–26. [PubMed: 20643221]
58. Ohya T, et al. Reconstitution of Rab- and SNARE-dependent membrane fusion by synthetic endosomes. Nature. 2009; 459:1091–1097. [PubMed: 19458617]

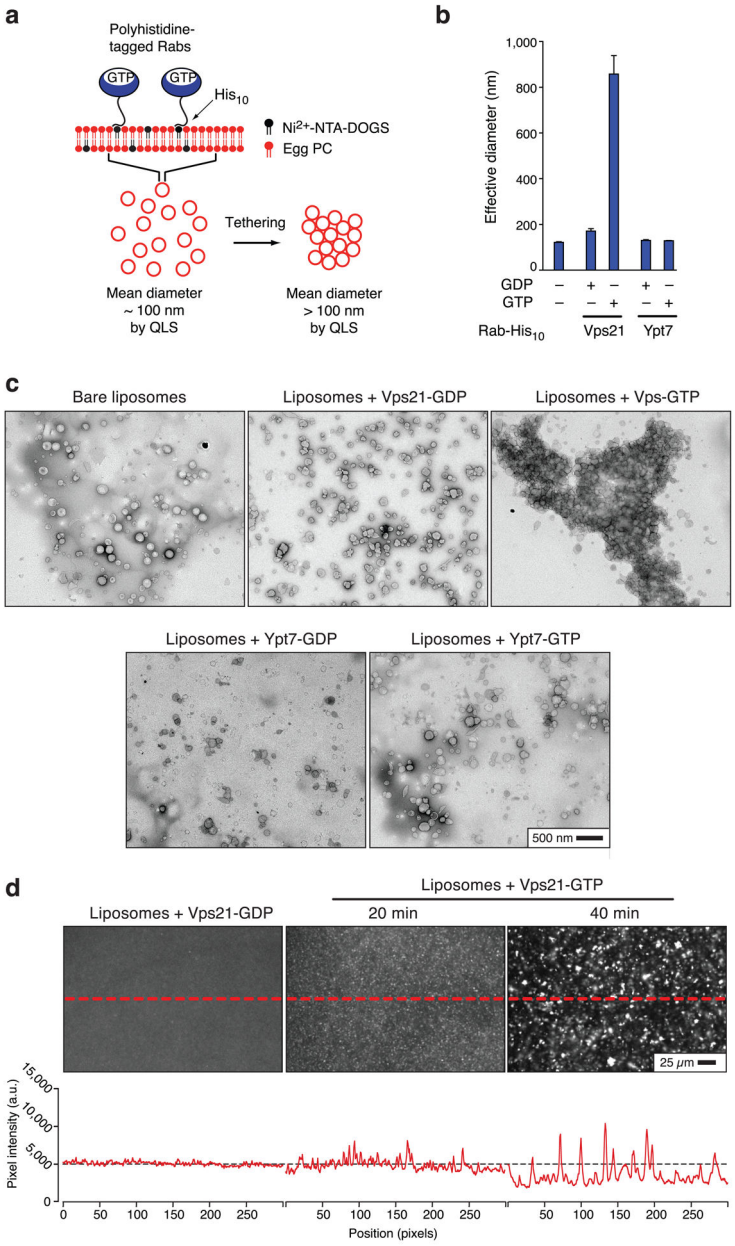

Fig. 1.

GTP-bound Vps21 tethers liposomes. **(a)** Experimental configuration. Full details are presented in the Methods and Supplementary Methods sections. **(b)** Liposome particle size distributions were measured by QLS after a 60 min incubation in the presence of the indicated Rab-His_{10} proteins, preloaded with GDP or GTP. Bars indicate mean and s.e.m. for 3 independent experiments. **(c)** TEM images of negatively stained samples taken from the experiment shown in panel b. **(d)** Liposomes were prepared as for parts a–c, except that Texas Red-labeled phosphatidylethanolamine lipid was incorporated. Fluorescent liposomes with GDP- or GTP-loaded His_{10}-Vps21 were incubated for 20 or 40 min, and then a drop of the suspension was placed between two class coverslips and imaged by epifluorescence

microscopy (10× objective, 200 ms exposure). Brightness and contrast adjustments were identical for the three panels shown. Traces below the images show pixel intensities along the indicated line segments (dashed lines). Individual liposomes in the starting population are too small, and diffuse too rapidly, to be individually resolved under these conditions, and appear as diffuse fluorescence. Note that as tethering proceeds, the clusters grow in size and the fluorescent background markedly decreases, indicating that most of the individual liposomes in the population have entered into the tethered clusters. Images of liposomes decorated with GDP- His_{10}-Vps21 are shown at 20 min incubation, and were indistinguishable from 40 min incubation.

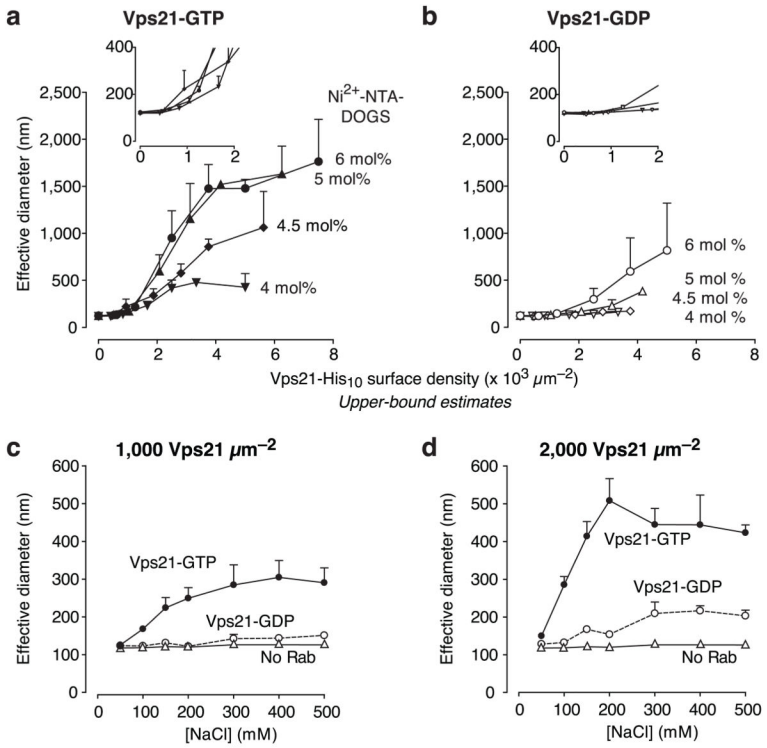

Fig. 2.

Vps21 surface density and tethering activity. **(a** and **b)** Liposome tethering, measured by QLS, was examined as a function of Vps21 membrane surface density. Vps21 was loaded with (**a**) GTP or with (**b**) GDP. Insets show the onset of tethering at low Vps21 surface densities. Additional surface density data for Vps21 and Ypt7 are shown in Supplementary Fig. S1. **(c** and **d)** To test the effect of ionic strength, liposomes were decorated with Vps21-GDP or -GTP at two different surface densities, and tethering was monitored by QLS in buffers containing the indicated salt concentrations. As in (a) and (b), the indicated Vps21 surface densities are upper-bound estimates. Bars indicate mean and s.e.m. from 3 independent experiments.

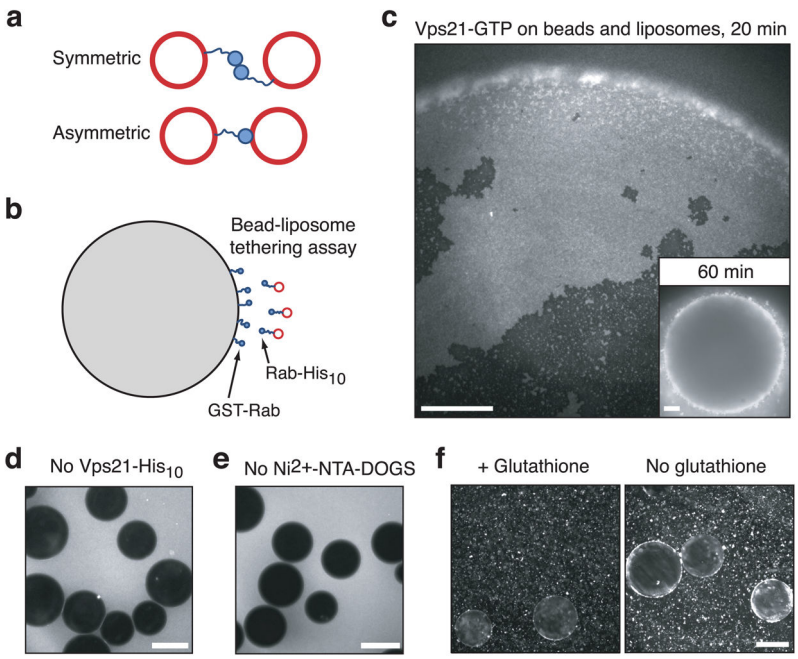

Fig. 3.

Vps21 interactions *in trans* are required for efficient tethering. **(a)** Schematic diagram showing two possible mechanisms of Rab-mediated tethering. **(b)** Schematic diagram of the bead-liposome tethering assay. **(c)** GTP-loaded GST-Vps21 beads were photographed after incubation for 20 or 60 min in the presence of fluorescent liposomes containing 6 mol% Ni^{2+}-NTA-DOGS and GTP-loaded Vps21-His_{10}. Images are representative of nine independent experiments. Scale bars = 15 μm (a) and 75 μm (b–d). **(d)** As in panel a inset, but without GTP-loaded Vps21-His_{10}. **(e)** As in panel a inset, but liposomes were prepared without Ni^{2+}-NTA-DOGS. **(f),** As in panel a, except that after a 20 min incubation, 10 mM reduced glutathione was added (left panel), or buffer without glutathione was added (right panel). Samples were then incubated for 4 min more, and photographed.

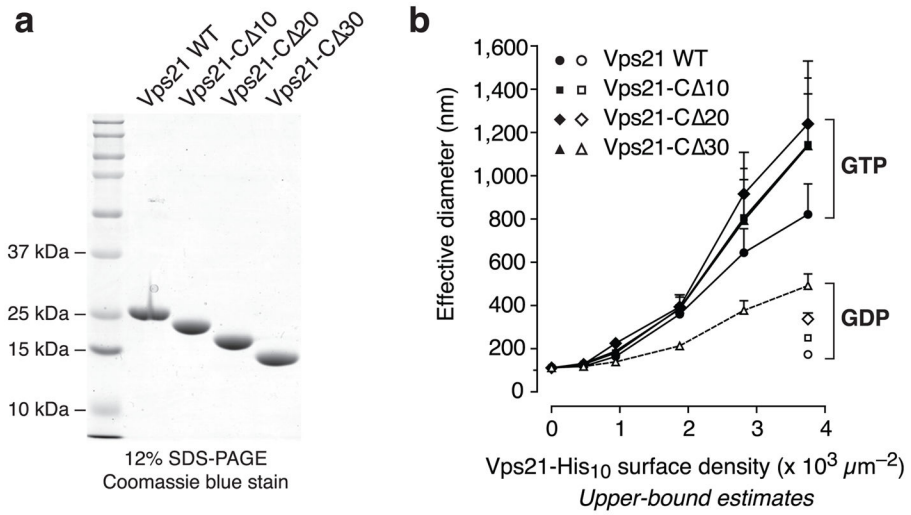

Fig. 4.

The Vps21 C-terminal linker is not required for tethering. **(a)**Vps21-His_{10} fusion proteins lacking the last 10, 20, or 30 residues of the Vps21 C-terminal linker were prepared. The purified proteins (5 μg) were analyzed by SDS-PAGE. **(b)** Liposomes bearing these proteins were assayed by QLS for the ability to drive tethering over the indicated range of surface densities. Each construct was loaded with either GTP (filled symbols) or GDP (open symbols). Liposomes contained 4.5 mol % Ni^{2+}-NTA-DOGS. Bars indicate mean and s.e.m. from 4 independent experiments.

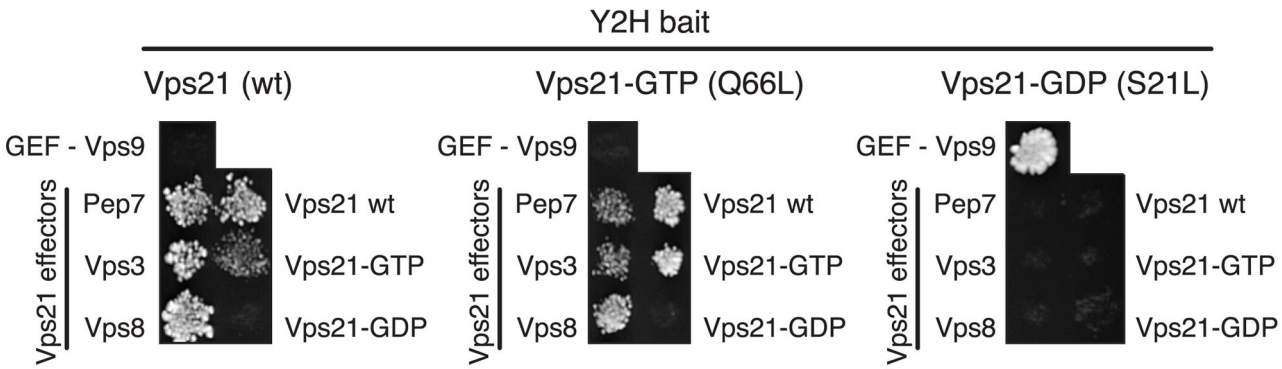

Fig. 5.

Vps21-GTP interacts with known effectors and with itself in Y2H assays. A positive interaction in the Y2H assay is indicated by yeast colony growth on medium lacking Trp, Leu and His, and supplemented with 1.5 mM 3-aminotriazole. The Vps21 effectors Vac1 (a.k.a. Pep7), Vps3, and Vps8 are positive controls for interaction selectivity with Vps21-GTP, while Vps9 is a control for interaction selectivity with Vps21-GDP.

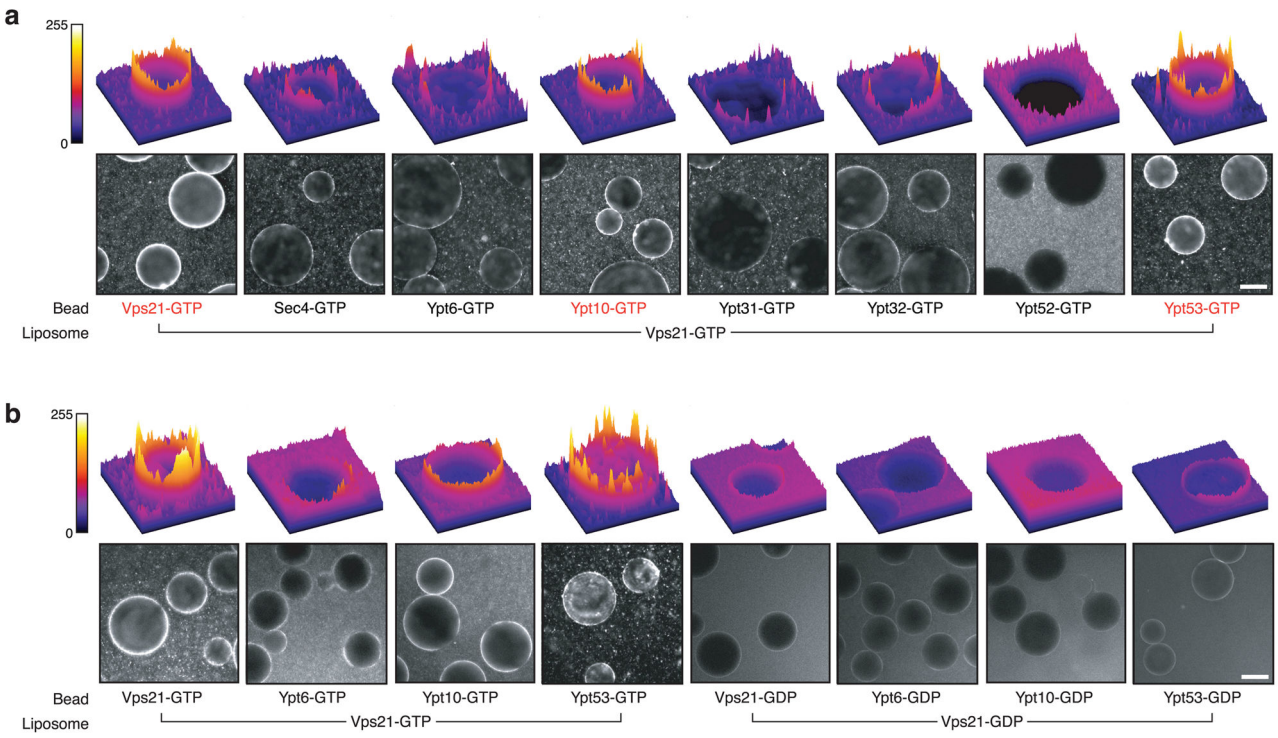

Fig. 6.

Vps21 interacts with Ypt53 and Ypt10 to drive GTP-dependent heterotypic tethering. **(a)** Heterotypic Rab-Rab tethering was assayed as in Fig. 2a–f, except that beads were decorated with various GTP-loaded GST-Rab fusion proteins, as indicated. The bottom panels in each set show representative fields of beads under epifluorescence illumination. The top panels show fluorescence intensity profile plots of representative beads. **(b)** Assays were performed as in panel a, except that the Rabs were preloaded with either GTP or GDP, as indicated. Ypt6, which does not interact with Vps21, served as a negative control. Scale bars = 75 μm.

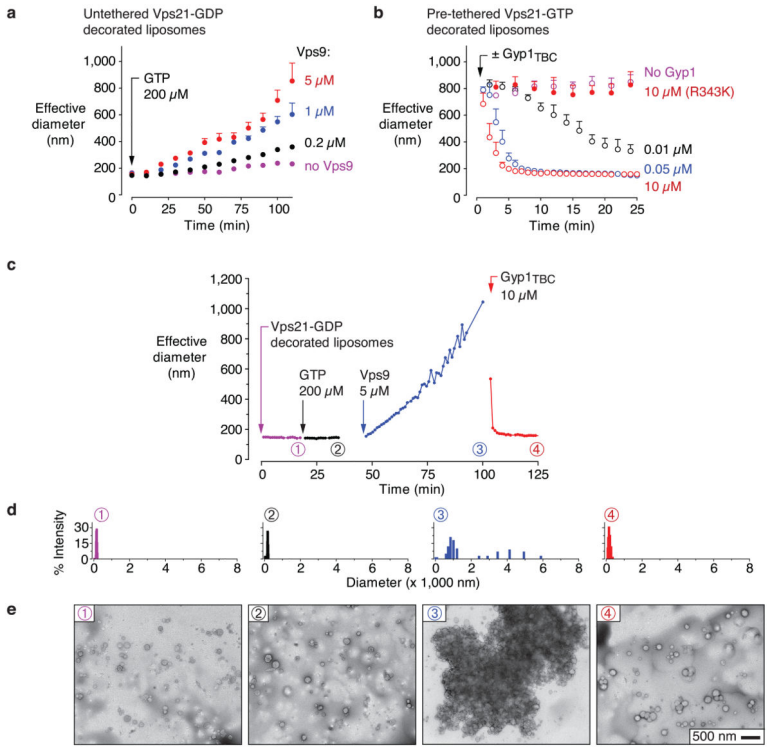

Fig. 7.

Regulation and reversibility of Vps21-mediated liposome tethering. **(a)** GEF-stimulated tethering. Tethering by GDP-loaded Vps21-decorated liposomes was measured by QLS following the addition of 0.2 mM GTP and varying concentrations of Vps9. Bars span mean + s.e.m.; data points from three independent experiments were binned into 10 min intervals. **(b)** GAP-mediated reversal of tethering. GTP-loaded Vps21-decorated liposome tethering was measured by QLS following the addition of $Gyp1_{TBC}$ or (*) $Gyp1_{TBC\text{-}R343K}$. Bars span mean + s.e.m.; data from three independent experiments were binned into 2 min intervals. **(c)** Regulated cycle of tethering and de-tethering. Vps21-mediated liposome tethering, measured by QLS, was examined during sequential addition of 0.2 mM GTP, 5 μM Vps9, and 10 μM $Gyp1_{TBC}$. The data shown are representative of three independent experiments. **(d)** Histograms of Vps21-decorated liposome size distributions, derived from QLS, at the time points indicated in panel c. **(e)** TEM images of negatively stained samples withdrawn at the indicated time points from the experiment analyzed in panels c and d.

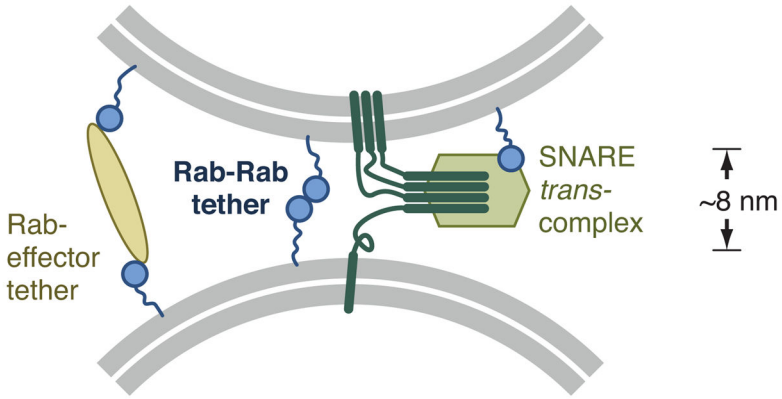

Fig. 8.

Model for Rab-Rab driven tethering in endosome docking and fusion. In this working model, three representative Rab functions are shown: classical effector-mediated tethering, Rab-Rab tethering, and coordination of *trans*-SNARE complex assembly by a Rab-mediated recruitment of a SNARE-binding regulator. Together, these mechanisms could in principle coordinate an ordered tethering, docking and fusion sequence.